J Eng Math
DOI 10.1007/s10665-016-9846-x

New analytical solutions for static two-dimensional droplets under the effects of long- and short-range molecular forces

J. R. Mac Intyre · J. M. Gomba · Carlos A. Perazzo

Received: 23 June 2015 / Accepted: 11 January 2016

Abstract We report new analytical solutions for the thickness profile of partially wetting two-dimensional droplets. The model includes the effects of capillarity and both short- and long-range molecular forces. We analyze the dependence of the maximum thickness, the contact angle, and the cross-sectional area on the height of the nanometric precursor film that surrounds the droplet. We found asymptotic expressions for the thickness profile and for the contact angles for large and small droplets. The results are compared to those obtained previously for polar liquids. The analytical solutions found here are useful to assess the validity of the hypothesis and the semi-analytical solutions proposed in the literature. In addition, these solutions enable the inference of information about the molecular potential from the measured steady profiles.

Keywords 2D droplet · Contact angle · Disjoining/conjoining pressure · Partial wetting

1 Introduction

The analyses of droplets and thin films are receiving considerable attention in both fundamental and in applications fields [1–3]. New techniques for imaging and production of droplets make it possible to obtain detailed thickness profiles of micro- and nano-droplets [4,5]. This precise information is useful to test theoretical models that relate morphological parameters, such as the contact angle, the thickness of the precursor film, or the position of the inflection points, with parameters related to the molecular interaction between the solid and the fluid, such as the Hamaker and dielectric constants [6,7]. These parameters are essential to understand the wetting properties of liquids and to chemically characterize the interfaces.

The molecular forces between the solid and the liquid are remarkably important at small scales and have a noticeable effect on the thickness profile of droplets. Classical solutions, such as cylindrical or spherical shapes, have failed to quantitatively account for certain features of flows at the micro- and nano-scales (see, e.g., [2,3]). Thus,

J. R. Mac Intyre (✉) · J. M. Gomba
Instituto de Física Arroyo Seco, CIFICEN, Universidad Nacional del Centro de la Provincia de Buenos Aires, Pinto 399, 7000 Tandil, Argentina
e-mail: jmintyre@exa.unicen.edu.ar

C. A. Perazzo
Dep. de Física y Química, FICEN, Universidad Favaloro, Tte. Gral. J. Perón 3175, Buenos Aires, Argentina
e-mail: perazzo@favaloro.edu.ar

Published online: 19 February 2016

more research is needed to better understand the physics of microflows and improve the efficiency of microfluidic systems where the actions of molecular and interfacial forces play a key role. In other words, "a well-founded understanding of equilibrium behavior is a prerequisite for the accurate modeling of the dynamic contact line behavior" [8].

The interaction between the solid and fluid molecules is usually modeled in terms of a disjoining–conjoining pressure which takes into account the action of two antagonistic molecular forces [9], such as electrostatic forces between charged surfaces, dispersion forces, interactions due to layers of neutral molecules adsorbed on the two surfaces, structural effects of the solvent, among others. In a previous work, one of our group collaborated in the development of a method that allows to find, for the first time, analytical solutions for the thickness profile h of two-dimensional droplets under the effect of antagonistic molecular forces [10]. This work was extended in Ref. [11] by including the effect of gravity. The molecular forces analyzed in those articles model London–van der Waals and ionic-electrostatics interactions [12–14]. In particular, the ionic-electrostatic component is present in liquids (in general, water solutions) with dissolved ions that can attach to a solid substrate. Thus, it is basically a solid–fluid interaction. Its dependence on h^{-2} was confirmed in experiments with *polar* liquids on glass [15,16].

Here, we present new analytical solutions for the shape of a droplet of a *non-polar* liquid and compare them with previous results, particularly with those in Ref. [10]. The disjoining–conjoining pressure that we use in the present article has been largely employed to model the competition between retarded and non-retarded effects of London–van der Waals interactions when the electrostatic component is not present [17–25]. Experiments with non-polar films on metals and glasses agree with the theoretically proposed terms [15,16,26]. In particular, the attractive term of the potential results from considering the London–van der Waals non-retarded molecular interactions, and it is employed in combination with different repulsive terms, as discussed below.

The equation for the shape of a static droplet has been solved by means of numerical methods [27,28], series expansions valid in the region where the liquid–vapor interface meets the substrate [29,30], asymptotic matching [19,21,31], ellipsoidal droplet modeling [32] and parametric solutions [33]. A remarkable difference with these results is that our solution describes the shape of the droplet from the maximum to the nanometric film by a single expression. Moreover, our analytical solutions have advantages over numerical ones. First, they explicitly show the relationships between geometrical and chemical parameters which is one of the goals of the present work. We show how the thickness of the film surrounding the droplet, h_{f}, the contact angle, the maximum thickness, etc, are determined by the size of the droplet and the combined strength of the molecular forces, i.e., with the Hamaker constants, surface tension, and the minimum of the molecular potential. Second, they are useful to verify and test numerical codes. Third, when the ratio of the maximum height to the precursor film thickness increases, the use of realistic values for h_{f} (about 10–100 nm) in problems with moving contact lines is impractical because it requires cell sizes of the order of h_{f} (see for example Refs. [34,35]). Then, the static droplet profiles are a good alternative to describe moving droplets that almost do not change their shape in time, as occurs (for certain range of parameters) in the thermocapillary flow of droplets [29,36].

This article is organized as follows. In Sect. 2, we present the basic equations. In Sect. 3, we establish the parameter ranges that allow static droplet solutions. Section 4 presents a new analytical solution for the shape of the droplet, asymptotic analyses for small and large droplets, and a comparisons with previous results. The dependence of the cross-sectional area, A, and the contact angle, θ, on h_{f} and on the disjoining–conjoining potential is presented in the first subsection of Sect. 5. In a subsequent subsection, we discuss the morphology of the droplets in terms of A. Finally, we present the conclusions.

2 Mathematical model

Let us to consider a plane substrate covered by a liquid layer with thickness $h \equiv h(x,t)$, viscosity μ and surface tension γ, being x and z the coordinates along and normal to the substrate, respectively (see Fig. 1). Under the lubrication hypothesis, the thickness of the profile must be much smaller than its extension so that it is possible to perform a perturbation series in powers of the small aspect ratio. Assuming that the Reynolds number satisfies

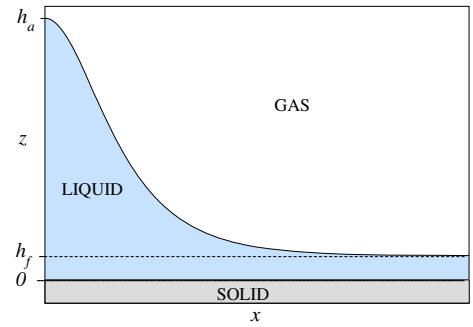

Fig. 1 Definition of variables. The thickness of the precursor film h_f is the control parameter of the problem

Re $\sim \mathcal{O}(1)$, the continuity and the Navier–Stokes equations are simplified to a partial differential equation that describes the evolution of $h(x,t)$ [37]:

$$\frac{\partial h}{\partial t} + \frac{\partial (hu)}{\partial x} = 0, \tag{1}$$

$$u = \frac{h^2}{3\mu}\frac{\partial}{\partial x}\left[\gamma \frac{\partial^2 h}{\partial x^2} + \Pi(h)\right], \tag{2}$$

where $u \equiv u(x,t)$ is the mean velocity (averaged in z) in the x direction. The term with γ models the capillarity and Π is the disjoining–conjoining pressure, which takes into account the molecular interaction between the liquid and the substrate [9,13].

The model for $\Pi(h)$ that we employ is [14,20,23,36,38,39],

$$\Pi(h) = \kappa\left[\left(\frac{h_*}{h}\right)^n - \left(\frac{h_*}{h}\right)^m\right], \tag{3}$$

which represents the competition between two antagonistic molecular forces. Here, we present new analytical solutions for the case $(n,m) = (4,3)$. The parameter κ is proportional to the Hamaker constant [10], and h_* is the minimum of the potential U defined as

$$U(h) = -\int \Pi(h)\, \mathrm{d}h. \tag{4}$$

The definition in Eq. (3) is largely-employed to model the effects of molecular interactions. The case $(n,m) = (3,2)$, analyzed in Ref. [10], represents the competition of London–van der Waals ($n = 3$) and ionic-electrostatics forces ($m = 2$) [12,36,38]. The dependence with $m = 2$, valid for thickness much lower than the Debye length [15,26], was verified in experiments of water films on glass, quartz and mica [16]. The term with $m = 3$ is an exact classical result obtained by summing individual London–van der Waals interactions between molecules. This term has been combined with a second term with opposite sign to avoid the films to collapse. The choice $n = 9$, originated from the repulsive Lennard-Jones interaction [38,39], has been criticized because repulsive intermolecular interactions led, on the contrary, a net attraction between the free interface and the substrate [31]. A potential with $n = 6$ has been derived by Pismen in the long-scale limit of a diffuse interface theory with application to layers thicker than the molecular scales. Here we employ $n = 4$, perhaps one of the most popular choices [18,19,21,22,24,40,41]; this term is an exact expression that results from considering retardation effects in London–van der Waals interactions [15,23,42]. Experiments with tetradecane on quartz and hexane on metal have shown that the exponents (4, 3) correctly describe retarded and non-retarded effects in London–van der Waals interactions.

To simplify the analysis, we define the following dimensionless variables

$$\hat{h} = \frac{h}{h_*}, \quad \hat{x} = \frac{x}{x_c}, \quad \hat{t} = \frac{\gamma h_*^3}{3\mu x_c^4} t, \quad x_c^2 = \frac{\gamma h_*}{\kappa}. \tag{5}$$

Replacing them in Eqs. (1) and (2) and omitting the hats, the evolution equation becomes

$$\frac{\partial h}{\partial t} + \frac{\partial}{\partial x}\left[h^3 \frac{\partial^3 h}{\partial x^3}\right] + \frac{\partial}{\partial x}\left[h^3 \frac{\partial}{\partial x}\left(\frac{1}{h^n} - \frac{1}{h^m}\right)\right] = 0. \tag{6}$$

We kept the temporal term up to this point to show that the chosen scales in Eq. (5) results in a parameter-free equation, even in the case of moving droplets.

3 First integral and space solution

Requiring that $u = 0$ and integrating once, we get an equation that rules the shape of static droplets:

$$\frac{\mathrm{d}^2 h}{\mathrm{d}x^2} + \left(\frac{1}{h^4} - \frac{1}{h^3}\right) = -P; \quad P = -h_\mathrm{f}^{-4} + h_\mathrm{f}^{-3}, \tag{7}$$

where the value of P results from requiring a zero curvature at the film region of thickness h_f. Integrating Eq. (7) and requiring a vanishing first derivative at $h = h_\mathrm{f}$, the following expression is obtained:

$$h_x^2 = \frac{2(h - h_\mathrm{f})^2}{h_\mathrm{f}^4 h^3}(h - h_\mathrm{a})(h - h_\mathrm{b})(1 - h_\mathrm{f}), \tag{8}$$

$$h_\mathrm{a} = \frac{4h_\mathrm{f} - 3h_\mathrm{f}^2 + h_\mathrm{f}\Delta}{12(h_\mathrm{f} - 1)}, \tag{9}$$

$$h_\mathrm{b} = \frac{4h_\mathrm{f} - 3h_\mathrm{f}^2 - h_\mathrm{f}\Delta}{12(h_\mathrm{f} - 1)}, \tag{10}$$

$$\Delta = \sqrt{-32 + 24h_\mathrm{f} + 9h_\mathrm{f}^2}. \tag{11}$$

A solution of Eq. (8) describing a droplet in contact with a flat precursor film requires null slope at $h = h_\mathrm{f}$ and at the top of the droplet. Since $h_\mathrm{b} < 0$ for $h_\mathrm{f} > 0$, then the maximum of the drop is h_a, and in consequence $h_\mathrm{f} < h_\mathrm{a}$. Real positive values for h_a implies $h_\mathrm{f} > 1$, and $h_\mathrm{f} < h_\mathrm{a}$ implies $h_\mathrm{f} < 4/3$. Then, Eq. (8) has a droplet solution if

$$1 < h_\mathrm{f} < \frac{4}{3}. \tag{12}$$

The minimum allowed value for h_f is the same as in Ref. [10]. Given that if $(n, m) = (3, 2)$ the upper bound is $3/2$ [10] and for $(n, m) = (4, 3)$ is $4/3$, one may speculate that this maximum value is n/m. Nevertheless, applying the same procedure for $(n, m) = (9, 3)$ (employed, for example, in Ref. [39]), we obtain that the maximum value is $3^{1/6}$. To clarify this point, we observe that the flat film surrounding a stable droplet must be stable [11]. The energy, per unit length, of flat a film with dimensional thickness b is

$$\varepsilon = \gamma + \gamma_\mathrm{SL} + U(b), \tag{13}$$

where γ_SL is the energy per unit length at the solid–liquid interface. To have a minimum of energy, and then a stable film, the second derivative of ε must be positive, which together Eq. (3) give

$$\frac{b}{h_*} < \left(\frac{n}{m}\right)^{1/(n-m)}. \tag{14}$$

Notice that the upper boundary given in Eq. (14) also corresponds to the minimum of Π. This thickness has an interesting property: it is the height at which large droplets ($h_\mathrm{f} \to 1$) present the maximum curvature. This information is useful to infer, from a detailed experimental profile, the value of the minimum of the molecular potential and, consequently, the maximum value for the precursor film.

4 Droplet profile

In order to obtain an expression for the thickness profile, we integrate Eq. (8), that is,

$$x = \pm \int \frac{h_\mathrm{f}^2 h^{3/2}\,\mathrm{d}h}{(h-h_\mathrm{f})\sqrt{2(h_\mathrm{a}-h)(h-h_\mathrm{b})(h_\mathrm{f}-1)}}. \tag{15}$$

We find an analytical solution given by

$$x = \pm(F_1 + F_2 + F_3), \tag{16}$$

where we define the quantities F_1, F_2, F_3 as

$$F_1 = \alpha \mathrm{E}\left(\arcsin\left(\psi\sqrt{h_\mathrm{a}-h}\right), M_+\right), \tag{17}$$

$$F_2 = \beta\left[\mathrm{F}\left(\arcsin\left(\psi\sqrt{h-h_\mathrm{b}}\right), M_-\right) - \mathrm{K}(M_-)\right], \tag{18}$$

$$F_3 = \lambda\left[\tilde{\Pi}\left(\chi, \arcsin\left(\psi\sqrt{h-h_\mathrm{b}}\right), M_-\right) - \tilde{\Pi}(\chi, M_-)\right], \tag{19}$$

with

$$\chi = \frac{2\Delta}{\delta}, \quad \delta = -16 + 15h_\mathrm{f} + \Delta, \tag{20}$$

and

$$\psi = \sqrt{\frac{6(h_\mathrm{f}-1)}{h_\mathrm{f}\Delta}}, \quad M_\pm = \frac{2\Delta}{\pm(4-3h_\mathrm{f}) + \Delta}. \tag{21}$$

The functions $\mathrm{F}(\phi, k)$, $\mathrm{E}(\phi, k)$, and $\tilde{\Pi}(n, \phi, k)$ are incomplete elliptic integrals of the first, second, and third kinds, respectively, and $\mathrm{K}(k) = \mathrm{F}(\pi/2, k)$ and $\tilde{\Pi}(n, k) = \tilde{\Pi}(n, \pi/2, k)$ are complete elliptic integrals of the first and third kind respectively [43], and α, β and λ are defined as follows:

$$\alpha = -h_\mathrm{f}^2\sqrt{\frac{2h_\mathrm{a}}{h_\mathrm{f}-1}}, \tag{22}$$

$$\beta = \mathrm{i}h_\mathrm{f}^2\sqrt{6h_\mathrm{a}}, \tag{23}$$

$$\lambda = -\frac{12(h_\mathrm{f}-1)}{\delta}\beta. \tag{24}$$

Equation (16) is a stationary solution of Eq. (7) describing the thickness profile h of a two-dimensional drop of a liquid with a disjoining–conjoining pressure as given in Eq. (3) with $n = 4$ and $m = 3$. This is the main result of this

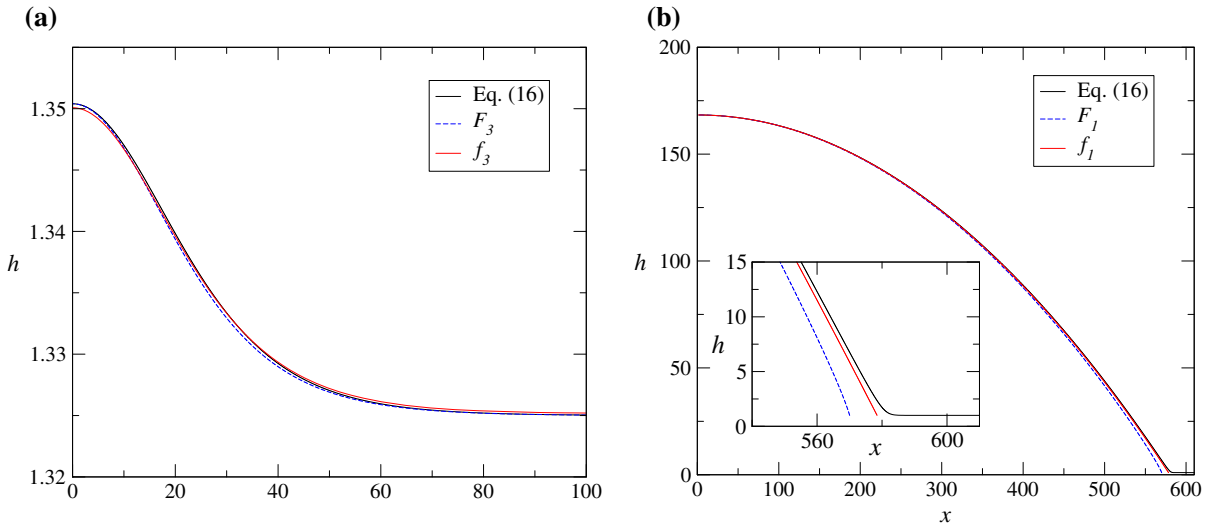

Fig. 2 (color online) Comparison between the closed solution given in Eq. (16) and the corresponding approximate expressions for **a** small droplets, here $h_\mathrm{f} = 1.325$, and **b** large droplets, here $h_\mathrm{f} = 1.001$

work, and it allows to study the properties of the droplet and to obtain relationships between different quantities, such as the nanometric thickness h_f, the contact angle, the cross-sectional area, and the maximum thickness.

Simpler expressions can be obtained for both small and large droplets. Small drops are obtained for $h_\mathrm{f} \to 4/3^-$. In this limit $F_1, F_2 \approx 0 + O(\sqrt{h_\mathrm{f} - 4/3})$ and then the profile is well represented by F_3. Taking the first order of the arguments of $\tilde{\Pi}$, F_3 can be simplified to f_3

$$f_3 = -\frac{16\mathrm{i}\sqrt{2}}{9}\left\{\tilde{\Pi}\left(1 - \frac{9}{8}\left(h_\mathrm{f} - \frac{4}{3}\right), \arcsin\left(\frac{\sqrt{8+6h}}{32}(4+3h_\mathrm{f})\right), 2\right) - \tilde{\Pi}\left(1 - \frac{9}{8}\left(h_\mathrm{f} - \frac{4}{3}\right), 2\right)\right\}. \tag{25}$$

Large drops are attained if $h_\mathrm{f} \to 1^+$, where $F_2, F_3 \ll F_1$. Taking the first order of the arguments of E and integrating, F_1 is reduced to

$$F_1 \to f_1 = -\sqrt{\frac{2(h_\mathrm{a} - h)}{h_\mathrm{f} - 1}} + O(h_\mathrm{f} - 1). \tag{26}$$

Notice that in this limit h is a quadratic function of x and the drop profile is a parabola. In Fig. 2, we compare these approximations with the complete solution given by Eq. (16) for two different values of h_f.

We compare the solution (16) with some approaches found in the literature. A key article on the study of stationary droplets is Ref. [40], where the authors make a rigorous mathematical analysis for different (n, m). Among other interesting results, they derive a leading-order solution of Eq. (7) valid for large droplets (a similar approach is employed in Ref. [19]). They distinguish three regions for the solution: 'the droplet', that corresponds to the macroscopic volume, the 'ultra-thin' film, where the solution is flat, and the 'interior layer', where the two previous regions meet. In our dimensionless variables, their 'droplet' solution is

$$h = \frac{h_\mathrm{f} - 1}{2}\left[\frac{1}{3(h_\mathrm{f} - 1)^2} - x^2\right]. \tag{27}$$

Identical expression is obtained by inverting f_1 in Eq. (26) and taking the first order expansion of h_a about $h_\mathrm{f} = 1$. The good agreement, for large droplets, between Eqs. (27) and (16) is shown in Fig. 2b. On the other hand, the

authors find that the 'ultra-thin' layer is given by $h_f = 1 + P$, a result that we can reproduce by expanding P, Eq. (7), about $h_f = 1$.

There are some approaches to describe the 'interior layer' or contact line region for large drops. In Ref. [29], it is assumed that, for $h > h_f$, U can be approximated only with the term proportional to h^{-2} (the one proportional to h^{-3} in Π). It is also assumed that the thickness of the precursor film is that which minimizes the potential (in the present context this implies that $h_f = 1$). To reproduce this procedure in our variables one has to set $P = 0$ and $dh/dx = 0$ for $h = h_f = 1$. Thus one obtains

$$h = \left(1 + (x - x_L)^2\right)^{1/2}, \tag{28}$$

being x_L a constant of integration that shifts the profile. In Ref. [44] an identical approach is followed but considering both the disjoining and conjoining terms. The exponents used in that work are $n = 5$ and $m = 3$ so that a direct comparison with our results is not possible. However, we follow the same procedure for $(n, m) = (4, 3)$ to obtain:

$$x - x_L = \sqrt{3h(h+2)} + \log\left(\frac{1 + 2h - \sqrt{3h(h+2)}}{h - 1}\right), \tag{29}$$

which describes the profile around the contact line for large drops. Taking the first order of Eq. (29) about $h = 1$ we obtain

$$h = 1 + C\mathrm{e}^{-x}, \tag{30}$$

being C a constant. This exponential dependence on x completely agrees with the results presented in Ref. [30], where the authors make an asymptotic study for the contact line region for any Π.

Figure 3 compares the profile in Eqs. (16) with (28) and (29). The physical reason for the inaccuracy of Eq. (28) to reproduce the profile is that the disjoining and conjoining terms are of the same order in the region $h \approx h_f$. This explains the difference in the steepness of this profile close to the flat film region. On the contrary, profiles in Eqs. (16) and (29) are in good agreement, strengthening the idea that both terms in the disjoining–conjoining pressure are relevant at the contact line region.

5 Comparative analysis: cases $(n, m) = (4, 3)$ and $(n, m) = (3, 2)$

Here we show that changing the exponents n and m may lead to remarkable differences between microscopic, and even macroscopic, observables. These differences are important to get information about the solid–liquid molecular potential from a given steady profile.

5.1 Contact angle and cross-sectional area

The contact angle θ describes the wettability of a liquid on a solid. It is determined by the affinity between the liquid and solid molecules, so it relates to the different parameters in the disjoining–conjoining pressure. We define θ as the angle of the interface at the inflection point, that is where $h_{xx} = 0$. There are four values that satisfy this equation. One is $h = h_f$, and only one of the other three has physical meaning for $1 < h_f < 4/3$. The thickness at the inflection point is

$$h_c = -\frac{h_f}{3} - \frac{2^{4/3}(h_f - 1)h_f^2}{3\,\omega} + \frac{2^{-1/3}\,\omega}{3(h_f - 1)}, \tag{31}$$

$$\omega^3 = (h_f - 1)^2\, h_f^3 \left(20 + 7h_f + 3\sqrt{48 + 3h_f(8 + 3h_f)}\right). \tag{32}$$

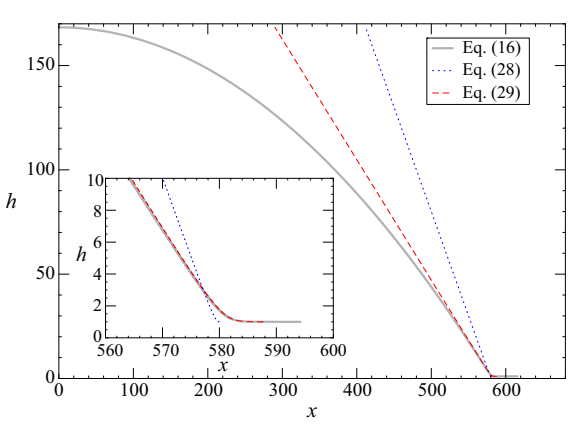

Fig. 3 (color online). Comparison of the complete analytical profile, Eq. (16), with the approximated expressions given in Eqs. (28) and (29). Here, $h_\mathrm{f} = 1.001$

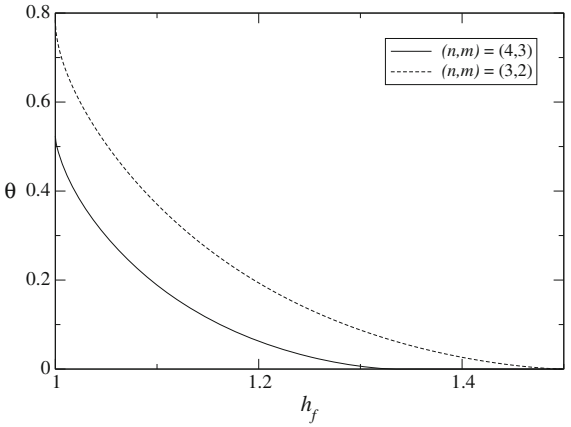

Fig. 4 Contact angle, in radians, as a function of h_f for $(n, m) = (4, 3)$ and $(n, m) = (3, 2)$

Replacing h_c in Eq. (8) we get the contact angle as an analytical function of h_f

$$\theta(h_\mathrm{f}) = \arctan\left(\sqrt{f(h_\mathrm{f})}\right), \tag{33}$$

$$f(h_\mathrm{f}) = \frac{\left((h_\mathrm{f}\,\omega\,\Delta)^2 - (h_\mathrm{f}^2\,\omega - 2y)^2\right)}{12\,h_\mathrm{f}^4\,\omega}\,\frac{(y + 8h_\mathrm{f}\,\omega(1-h_\mathrm{f}))^2}{(y + 2h_\mathrm{f}\,\omega(1-h_\mathrm{f}))^3}, \tag{34}$$

$$y = 2^{10/3}h_\mathrm{f}^3 - 2^{7/3}h_\mathrm{f}^4 + 2^{2/3}\omega^2 - 2^{7/3}h_\mathrm{f}^2. \tag{35}$$

Figure 4 shows θ versus h_f for $(n, m) = (4, 3)$ and $(n, m) = (3, 2)$. Interestingly, a given precursor film sustains a droplet with lower θ for the case with $(n, m) = (4, 3)$.

Since we use different scales to non-dimensionalize the x and z coordinates (see Eq. (5)), θ is different from the contact angle Θ of the droplet with the dimensions restored. They are related by means of the relationship $\tan\Theta = \sqrt{h_*\kappa/\gamma}\,\tan\theta$.

The area A above h_f of the droplet is obtained by integrating the thickness profile on the flat film. Although it is not possible to integrate analytically the elliptic integrals in Eq. (16), it is still possible to obtain an analytical expression for A by using Eq. (8)

$$\begin{aligned} A &= \int_{-\infty}^{\infty}(h - h_\mathrm{f})\,\mathrm{d}x = 2\int_{h_\mathrm{f}}^{h_\mathrm{a}}\frac{h - h_\mathrm{f}}{h_x}\mathrm{d}h \\ &= \frac{\sqrt{2}\,h_\mathrm{f}^2}{\sqrt{h_\mathrm{f}-1}}\left(\frac{2\,(2(h_\mathrm{a}+h_\mathrm{b})+h_\mathrm{f})}{3}\sqrt{\frac{(h_\mathrm{a}-h_\mathrm{f})(h_\mathrm{f}-h_\mathrm{b})}{h_\mathrm{f}}}\right. \\ &\qquad \left. - \frac{2\mathrm{i}\sqrt{h_\mathrm{a}}}{3}\Big(2(h_\mathrm{a}+h_\mathrm{b})(E(\varsigma,\tau)-E(\tau)) - (2h_\mathrm{a}+h_\mathrm{b})(F(\varsigma,\tau)-K(\tau))\Big)\right), \end{aligned} \tag{36}$$

where

$$\varsigma = \arcsin\left(\sqrt{\frac{h_\mathrm{a}}{h_\mathrm{f}}}\right), \quad \tau = \frac{h_\mathrm{b}}{h_\mathrm{a}}. \tag{37}$$

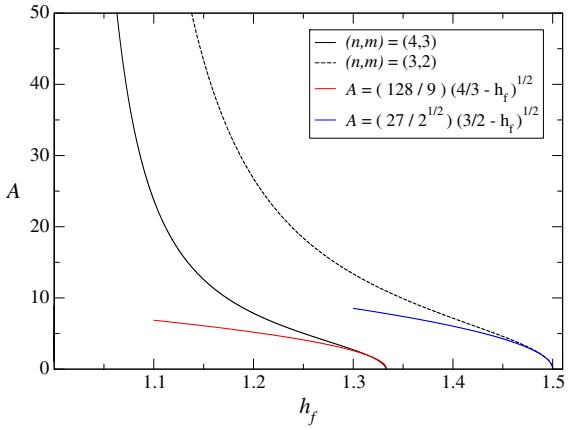

Fig. 5 (color online) Cross-sectional area versus h_f for $(n, m) = (4, 3)$ and $(n, m) = (3, 2)$. The *red* and *blue lines* correspond to the asymptotic dependence found for the small areas for the potentials with $(n, m) = (4, 3)$ and $(n, m) = (3, 2)$, respectively

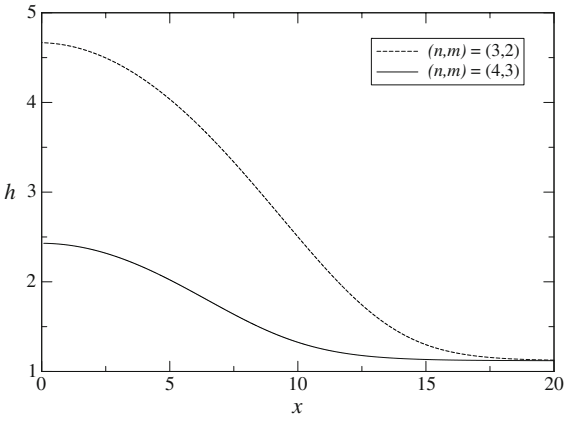

Fig. 6 Thickness profiles for $(n, m) = (4, 3)$ and $(n, m) = (3, 2)$ with $h_\mathrm{f} = 1.12$. The same precursor film sustains droplets with different contact angle and volumes

Figure 5 shows A versus h_f for the two cases. Interestingly, for a given value of h_f, the potential with $(n, m) = (4, 3)$ sustains a smaller droplet than the case with $(n, m) = (3, 2)$. Using the previously reported expression for A for the case $(n, m) = (3, 2)$ [10] and f_3 in Eq. (25) we find for small droplets that $A = c(n, m)(n/m - h_\mathrm{f})^{1/2}$ with $c(3, 2) = 27/\sqrt{2} \approx 19.09$ and $c(4, 3) = 128/9 \approx 14.2$. These relationships are of interest in the analysis of the dependence of the contact angle on the area, as we explain below.

Summarizing, we have found that for a given h_f, the case with $(n, m) = (4, 3)$ results in a droplet with a smaller contact angle and smaller area than the case with $(n, m) = (3, 2)$, as shown in the example of Fig. 6. To explain these features, we observe that for a given h_f in Eq. (3), the absolute value of the disjoining pressure is higher for case with $(n, m) = (3, 2)$ than for $(n, m) = (4, 3)$. A higher pressure at the film region must be compensated with a higher pressure in the non-flat region, a condition that is reached by increasing the curvature and consequently, θ and A.

5.2 Dependence of h_a and θ with A

Figure 7 shows the dependence of h_a on A. For both potentials, the maximum attains $A^{1/2}$ for large values of A. More surprisingly, the molecular forces have an appreciable effect on a macroscopic quantity as the maximum of the droplet even for large droplets. Notice that for the same large values of A, the maximum h_a is about 25 % larger for the case with $(n, m) = (3, 2)$ than for the case with $(n, m) = (4, 3)$.

In the limit of small drops (i.e., when h_f tends to its maximum), it can be shown that

$$h_\mathrm{a} = \frac{4}{3} + \frac{81A^2}{8192} \approx \frac{4}{3} + 0.01A^2 \quad \text{for } (n, m) = (4, 3), \tag{38}$$

$$h_\mathrm{a} = \frac{3}{2} + \frac{4A^2}{81} \approx \frac{3}{2} + 0.05A^2 \quad \text{for } (n, m) = (3, 2). \tag{39}$$

Thus, for a given A, the elevation over the precursor film, $h_\mathrm{a} - h_\mathrm{f}$, is approximately 20 % smaller for $(n, m) = (4, 3)$ than for $(n, m) = (3, 2)$.

Figure 8 compares the curves A vs θ for $(n, m) = (4, 3)$ and $(n, m) = (3, 2)$. For large A, both potentials attain a constant angle: $\theta \to \theta_* = \pi/6$ for $(n, m) = (4, 3)$, and $\theta \to \theta_* = \pi/4$ for $(n, m) = (3, 2)$. For small A, the angle θ for $(n, m) = (3, 2)$ is lower than for $(n, m) = (4, 3)$. In this limit, the simplified thickness profile

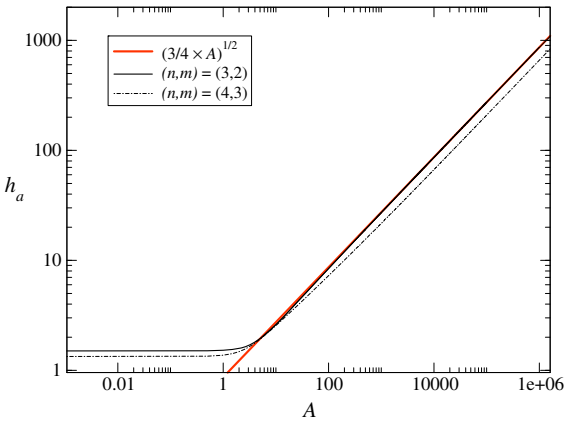

Fig. 7 Maximum h_a versus cross-sectional area A for $(n, m) = (3, 2)$ and $(n, m) = (4, 3)$. The potential law $(3/4 \times A)^{1/2}$ is derived from the analytical expression of A for the case $(n, m) = (3, 2)$, see Ref. [10]

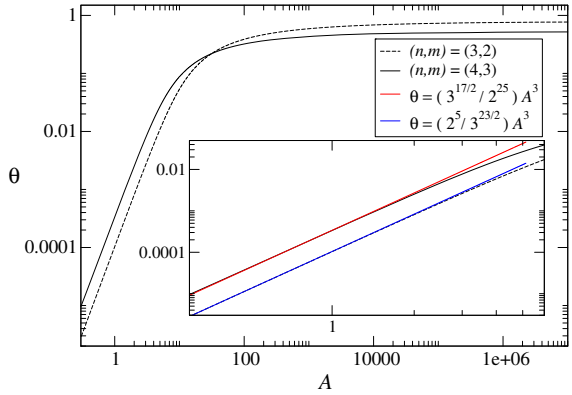

Fig. 8 (color online) Contact angle versus cross-sectional area for $(n, m) = (4, 3)$ and $(n, m) = (3, 2)$. For small volumes, the contact angle is higher for the potential with $(n, m) = (4, 3)$. The *red* and *blue lines* correspond to the asymptotic dependence found for the small areas for the potentials with $(n, m) = (4, 3)$ and $(n, m) = (3, 2)$, respectively

f_3 can be integrated giving $A \to 128/9(4/3 - h_f)^{1/2}$ and Eq. (33) gives $\theta \to 9\sqrt{3}/16(4/3 - h_f)^{3/2}$. Then, for $(n, m) = (4, 3)$ we obtain

$$\theta \to \frac{3^{17/2}}{2^{25}} A^3 \approx 3.4 \times 10^{-4} A^3 \quad \text{for } h_f \to \frac{4}{3}, \tag{40}$$

while for $(n, m) = (3, 2)$ the relationship is $\theta \to (2^5/3^{23/2})A^3 \approx 1.0 \times 10^{-4} A^3$. Notice that the power law dependence with A^3 suggests that it is independent of the pair (n, m). Interestingly, there is an area for which both potentials induce the same contact angle.

The analysis and conclusions of this section are valid in the dimensionless variables, and can be immediately extended to the dimensional space only when the vertical and horizontal scales of both potentials are the same, i.e., $h_{*(3,2)} = h_{*(4,3)}$ and $x_c = x_{c(3,2)} = x_{c(4,3)}$. It is instructive to visualize a case where the scales are not the same. For example, assuming that the asymptotic (large droplets) contact angle Θ_* of the dimensional profile is the same for both potentials, we ensure that the macroscopic physics is the same, while the microscopic origin of the potential is different. From Eqs. (5, 51) and considering $h_{*(3,2)} = h_{*(4,3)}$, we have that $x_{c(3,2)} = \sqrt{3} x_{c(4,3)}$. Thus, this comparison can be carried out by rescaling the curves that correspond to the potential (3,2) in Figs. 4, 5, 6, 7 and 8 by

$$x \to \sqrt{3}x; \quad A \to \sqrt{3}A; \quad \theta \to \arctan\left(\frac{1}{\sqrt{3}} \tan\theta\right). \tag{41}$$

Figure 9 shows how these rescalings modify Fig. 8. The asymptotic contact angle for large droplets is the same, but as A is reduced, the contact angle for $(n, m) = (3, 2)$ becomes smaller than for the case $(n, m) = (4, 3)$.

Figure 10 shows the comparison of two profiles that have the same asymptotic contact angle but different (n, m). The case $(3, 2)$ was rescaled according to Eq. (41). For large areas, the droplets are almost identical. As the area is decreased, the profile for $(n, m) = (3, 2)$ has smaller maximum thickness and contact angle than those for $(n, m) = (4, 3)$.

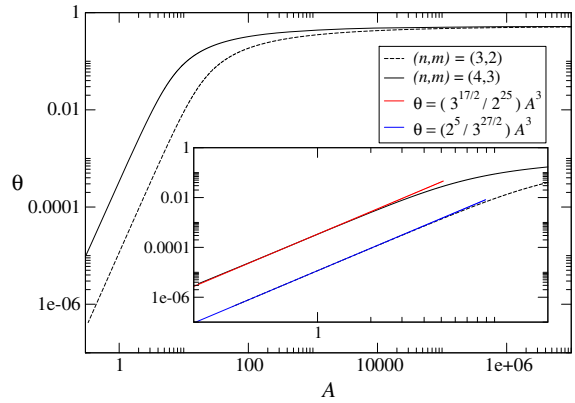

Fig. 9 (color online) Contact angle versus cross-sectional areas for $(n, m) = (4, 3)$ and $(n, m) = (3, 2)$, as presented in Fig. 8 but using the rescaling proposed in Eq. 41

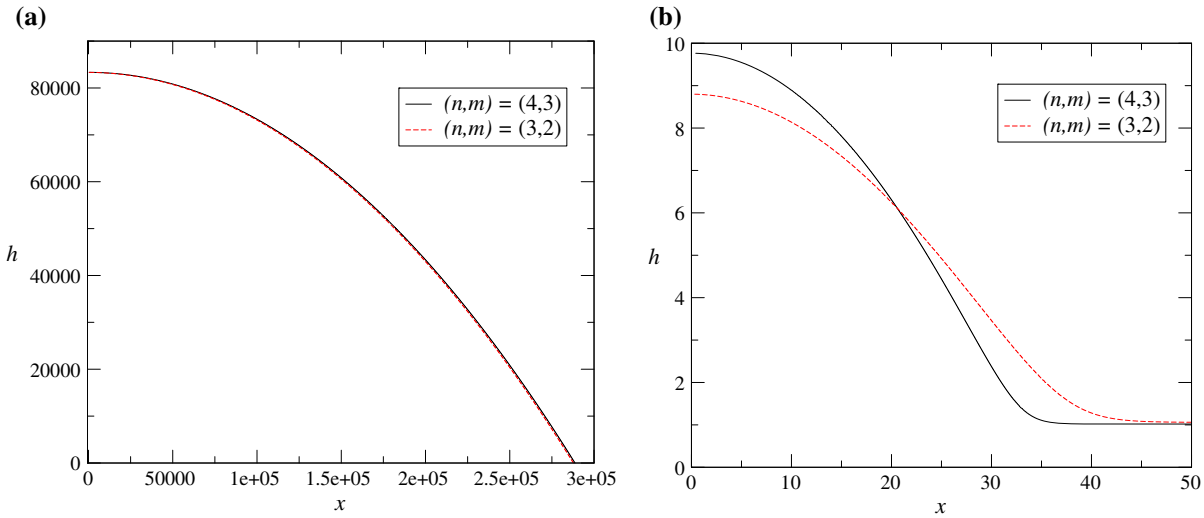

Fig. 10 (color online) Comparison between profiles with $(n, m) = (4, 3)$ and $(n, m) = (3, 2)$. The drops have the same h_* and Θ_*. **a** Large drop, $A = 3.2 \times 10^{10}$, and **b** small drop $A = 377.1$. We employed the x_c corresponding to the case $(n, m) = (4, 3)$ for all the curves

6 Conclusions

We presented new analytical solutions for the profile of a droplet under the effect of a disjoining–conjoining pressure. This pressure represents the effect of two, long- and short-range, antagonistic molecular forces. Equation (16) accounts, in a single expression, for the shape of the droplet from the nanometric precursor film that surrounds the droplet to the maximum. A simple and novel analytical relationship between the maximum thickness of the droplet and the thickness of the precursor film is presented. We found that for the case with $(n, m) = (4, 3)$, the thickness of the precursor film is bounded: $1 < h_f < 4/3$. This result was generalized for any pair (n, m). We observe that for $h_f \to 1$, the droplet increases its volume, and for $h_f \to 4/3$ the droplet becomes flat.

The profile is given as the sum of three terms. While the term F_2 smoothly connects the contributions of F_1 and F_3, these two last terms account for different effects. As shown in Fig. 2b, F_1 is a good approximation for the 'droplet' region of large volumes, where the capillarity is dominant and the disjoining pressure is negligible. Nevertheless, F_1 does not describe the transition and precursor film regions. In contrast, F_3 provides the shape of the thickness profile of the contact line region and is a good approximation for small droplets, for which the disjoining pressure has an noticeable effect even at the maximum (see Fig. 2). We also present simplified versions of Eq. (16) for the limits of small and large drops.

We compared our exact solutions with approaches found in the literature. We observe that asymptotics methods employed in Ref. [40] correctly predict the shape for the 'droplet' and the 'ultra-thin film' regions in the limit of large droplets. In Refs. [30,44] the authors find asymptotic expressions for the contact line region, which agree with our results. These comparisons might give valuable insight on how to set up expansions for the 3D droplets, where analytical solutions are not available.

The pairs $(n, m) = (4, 3)$ and $(n, m) = (3, 2)$ are suitable to model non-polar and polar liquids, respectively. We find noticeable effects of the disjoining pressure on the profile. Interestingly, the contact angle depends on the volume of the droplet: only for large droplets, the contact angle keeps constant and equal to $\pi/6$ for the case $(n, m) = (4, 3)$—smaller than the value $\pi/4$ found for the case $(n, m) = (3, 2)$. In the limit of small drops, both potentials show a dependence on A^3, suggesting that this dependence could be valid for any n and m.

We defined θ as the maximum slope of the profile. It is interesting to compare our definition with a standard definition, Θ_s, employed in the literature [38,45]:

$$\frac{\tan^2(\Theta_s)}{2} = -\frac{U(h_*)}{\gamma}. \tag{42}$$

Using the definition of U given in Eq. (4), and considering that $\tan^2(\Theta) = h_*\kappa/\gamma \tan^2(\theta)$, where θ is merely the contact angle in our dimensionless space (as discussed in Sect. 5), Eq. (42) becomes

$$\frac{\tan^2(\theta_s)}{2} = \frac{n-m}{(n-1)(m-1)},$$

which gives $\theta_s = \pi/6$ for $(n, m) = (4, 3)$ and $\theta_s = \pi/4$ for $(n, m) = (3, 2)$. Thus, the usual definition Eq. (42) agrees with our results in the limit of large droplets. In other words, Eq. (42) gives an angle that can only be observed in the limit of large droplets. Our definition for the contact angle, which is employed in experimental works [46], correctly predicts the contact angle of large droplets and the maximum slope for smaller ones (see Appendix). It is worth mentioning that if we employed a full expression for the curvature, a term with $1 - \cos\theta_s$ would appear in the place of $\tan^2\theta_s/2$ in Eq. (42), which results in the well-known Young's equation. In Ref. [47], the authors show that the thermodynamic contact angle given by the Young's equation is the one observed in the limits of large droplets.

Finally, we may ask if a thick film, i.e., $h_f > 4/3$, can support a droplet on it. We observed that the restriction for droplet-like solutions, $h_f < 4/3$, is related with the stability of the film that surrounds the droplet. Effectively, a standard linear stability analysis predicts that a film of thickness H is unstable when

$$-H^3k^4 + H^{2-m}k^2m - H^{2-n}k^2n > 0, \tag{43}$$

where k is the wavenumber of normal modes. For infinite domains, as considered here, this implies that $H^{2-m}m - H^{2-n}n > 0$. Considering $(n, m) = (4, 3)$, the film is unstable when $H > 4/3$ and, then, will not be able to sustain a droplet. This result is fully compatible with the requirement for drop solutions $h_f < 4/3$ obtained independently in Sect. 3.

For finite domains, a flat film will be stable if the shortest unstable wavelength is larger than the size of the domain. The final state will depend on the volume of fluid, on the size of the container and, for some range of the parameters, on how the container is filled (hysteretic effects) [48,49]. Non-steady distributions of fluids breaks up into near-equilibrium droplets connected by a nanometric film that finally coalesce into a single droplet surrounded by a stable thin film [19,21]. This final stage is described by our analytical solutions.

Acknowledgments The authors gratefully acknowledge the funding supports via the CONICET Grants PIP No. 356 and PIP No. 299, and the ANPCyP Grant No. 2012-1707.

Appendix: Relationship between the contact angles Θ_s and Θ

In this study, we establish the connection between the thermodynamic definitions of the contact angle Θ_s, Eq. (42) and the contact angle Θ defined as the maximum slope of the dimensional profile (see Sect. 5.1). As we discussed in Sect. 6, $\Theta \to \Theta_s$ only in the limit of large droplets.

In the following, we return to the dimensional variables. Thus, Eq. (7) takes the form:

$$\gamma K = \frac{\mathrm{d}U(h)}{\mathrm{d}h} - P, \tag{44}$$

where $K = h_{xx}/(1+h_x^2)^{3/2}$ is the curvature, and P is an unknown constant [10,11]. Imposing that $K \to 0$ when $h \to h_\mathrm{f}$ (film region), the value of P is

$$P = -\Pi(h_\mathrm{f}). \tag{45}$$

We now integrate Eq. (44) from h_f to an arbitrary thickness H:

$$\gamma \int_{h_\mathrm{f}}^{H} K \,\mathrm{d}h + \int_{h_\mathrm{f}}^{H} \Pi(h)\,\mathrm{d}h = -\int_{h_\mathrm{f}}^{H} P\,\mathrm{d}h. \tag{46}$$

The three integrals in (46) can be calculated to get

$$\gamma(1-\cos\alpha(H)) = U(H) - U(h_\mathrm{f}) + (h_\mathrm{f} - H)P, \tag{47}$$

where the angle α is defined as the angle between the substrate and the profile at any h, i. e., $\tan\alpha(h) = h_x$.

Equation (47) shows that the angle α at any thickness H will depend on H and U. If we used $K = h''(x)$, valid under the lubrication hypothesis, the left-hand side of Eq. (47) would read $\gamma/2\tan^2\alpha(H)$.

Notice that the angle α evaluated at the point h_c, where the slope is maximum, is the contact angle of the dimensional profile Θ. Then, to show that the thermodynamic contact angle Θ_s is the limit of $\Theta = \alpha(h_\mathrm{c})$ for large droplets, we first evaluate Eq. (47) in $H = h_\mathrm{c}$

$$\gamma(1-\cos\Theta) = U(h_\mathrm{c}) - U(h_\mathrm{f}) + (h_\mathrm{f} - h_\mathrm{c})P. \tag{48}$$

We now consider large droplets by taking the limit $h_\mathrm{f} \to h_*$. From Eqs. (45,31), we have $\{U(h_\mathrm{c});\,(h_\mathrm{f}-h_\mathrm{c})P\} \to \{0;\,0\}$. Denoting $\Theta_* \equiv \Theta(h_\mathrm{c} \to \infty)$ we conclude that, in this limit, Eq. (48) becomes

$$\gamma(1-\cos\Theta_*) = -U(h_*), \tag{49}$$

which is the usual definition for the thermodynamic contact angle Θ_s [47]. The conclusion is that $\Theta_* \equiv \Theta(h_\mathrm{c} \to \infty) = \Theta_s$, and then Θ_s can only be observed in large droplets. As mentioned above, when the lubrication approximation is employed, the term $(1-\cos\Theta)$ is replaced by $1/2\tan^2\Theta$ as shown in Eq. (42). Moreover, from the analysis in Sect. 5.1, where we show that the maximum slope monotonically increases as h_f decreases, it is straightforward that the thermodynamic angle given in Eq. (49) is the upper limit of the observable contact angle Θ, as discussed in the Conclusions.

From Eq. (49), we may also relate the strength of the disjoining pressure κ with Θ_s, n, m, and γ. Effectively, since

$$U(h_*) = -\kappa\frac{h_*(n-m)}{(n-1)(m-1)}, \tag{50}$$

then

$$\kappa = \frac{\gamma(1-\cos\Theta_*)(m-1)(n-1)}{h_*(n-m)}. \tag{51}$$

Again, if the curvature is approached as h_{xx}, the factor $1-\cos\Theta_*$ is replaced by $1/2\tan^2\Theta_*$. In the References the interested reader will find many examples where this relationship between the contact angle and κ is employed. Remarkably, there is a simple relationship between the values of κ and h_* with the Hamaker constants of the molecular forces. If the disjoining–conjoining pressure is written as $\Pi = A_n/h^n - A_m/h^m$, where A_i is related to the Hamaker constant, then

$$h_* = \left(\frac{A_n}{A_m}\right)^{1/(n-m)} \tag{52}$$

and

$$\kappa = \left(\frac{{A_m}^n}{{A_n}^m}\right)^{1/(n-m)}. \tag{53}$$

which is explained in the Appendix of Ref. [10].

References

1. Bonn D, Eggers J, Indekeu J, Meunier J, Rolley E (2009) Wetting and spreading. Rev Mod Phys 81:739–805
2. Lai YH, Yang JT, Shieh DB (2010) A microchip fabricated with a vapor-diffusion self-assembled-monolayer method to transport droplets across superhydrophobic to hydrophilic surfaces. Lab Chip 10:499–504
3. Daunay B, Lambert P, Jalabert L, Kumemura M, Renaudot R, Agache V, Fujita H (2012) Effect of substrate wettability in liquid dielectrophoresis (ldep) based droplet generation: theoretical analysis and experimental confirmation. Lab Chip 12:361–368
4. Arscott S, Descatoire C, Buchaillot L, Ashcroft AE (2012) A snapshot of electrified nanodroplets undergoing Coulomb fission. Appl Phys Lett 100(7):074103
5. Roberts CC, Rao RR, Loewenberg M, Brooks CF, Galambos P, Grillet AM, Nemer MB (2012) Comparison of monodisperse droplet generation in flow-focusing devices with hydrophilic and hydrophobic surfaces. Lab Chip 12:1540–1547
6. Israelachvili JN (1992) Intermolecular and surface forces, 2nd edn. Academic Press, New York
7. Berim GO, Ruckenstein E (2004) On the shape and stability of a drop on a solid surface. J Phys Chem B 108:19330–19338
8. Nold A, Sibley DN, Goddard BD, Kalliadasis S (2014) Fluid structure in the immediate vicinity of an equilibrium three-phase contact line and assessment of disjoining pressure models using density functional theory. Phys Fluids 26(7):072001
9. Derjaguin B, Kusakov M (1936) Contact-line dynamics of a diffuse fluid interface. Izv Akad Nauk SSSR Ser Khim 5:741
10. Gomba JM, Homsy GM (2009) Analytical solutions for partially wetting two-dimensional droplets. Langmuir 25(10):5684–5691
11. Gomba JM, Perazzo CA (2012) Closed-form expression for the profile of partially wetting two-dimensional droplets under gravity. Phys Rev E 86(056):310
12. Gotkis Y, Ivanov I, Murisic N, Kondic L (2006) Dynamic structure formation at the fronts of volatile liquid drops. Phys Rev Lett 97(18):186101
13. Churaev NV, Sobolev VD (1995) Prediction of contact angles on the basis of the Frumkin–Derjaguin approach. Adv Colloid Interface Sci 61:1–16
14. Teletzke GF, Davis HT, Scriven LE (1987) How liquids spread on solids. Chem Eng Commun 55:41–82
15. Starov V, Velarde M, Radke C (2007) Wetting and spreading dynamics. Surfactant science series. CRC Press, Boca Raton
16. Derjaguin B, Churaev N (1974) Structural component of disjoining pressure. J Colloid Interface Sci 49(2):249–255
17. Derjaguin BV, Rabinovich YI, Churaev NV (1978) Direct measurement of molecular forces. Nature 272:313–318
18. Oron A, Bankoff SG (2001) Dynamics of a condensing liquid film under conjoining/disjoining pressures. Phys Fluids 13:1107–1117
19. Glasner KB, Witelski TP (2003) Coarsening dynamics of dewetting films. Phys Rev E 67:016302
20. Schwartz LW, Roy RV (2004) Theoretical and numerical results for spin coating of viscous liquids. Phys Fluid 16:569–584
21. Gratton MB, Witelski TP (2008) Coarsening of unstable thin films subject to gravity. Phys Rev E 77:016301
22. Gratton MB, Witelski TP (2009) Transient and self-similar dynamics in thin film coarsening. Physica D 238(23–24):2380–2394
23. de Gennes PG (1985) Wetting: statics and dynamics. Rev Mod Phys 57:827–863

24. Oron A, Bankoff S (1999) Dewetting of a heated surface by an evaporating liquid film under conjoining/disjoining pressures. J Colloid Interface Sci 218(1):152–166
25. Schwartz LW (1998) Hysteretic effects in droplet motions on heterogenous substrates: direct numerical simulations. Langmuir 14:3440–3453
26. Derjaguin B, Churaev NV, Muller V (1987) Surface forces. Springer, New York
27. Sur J, Witelski TP, Behringer RP (2004) Steady-profile fingering flows in Marangoni driven thin films. Phys Rev Lett 93(24):247803
28. Thiele U, Neuffer K, Bestehorn M, Pomeau Y, Velarde MG (2002) Sliding drops on an inclined plane. Colloids Surf A 206:87–104
29. Brochard-Wyart F, Di Meglio JM, Quere D, De Gennes PG (1991) Spreading of nonvolatile liquids in a continuum picture. Langmuir 7(2):335–338
30. Zhang X, Neogi P, Ybarra R (2002) Stable drop shapes under disjoining pressure: I. A hierarchical approach and application. J Colloid Interface Sci 249(1):134–140
31. Pismen LM, Eggers J (2008) Solvability condition for the moving contact line. Phys Rev E 78(056):304
32. Lubarda VA, Talke KA (2011) Analysis of the equilibrium droplet shape based on an ellipsoidal droplet model. Langmuir 27(17):10705–10713
33. Diaz ME, Fuentes J, Cerro RL, Savage MD (2010) An analytical solution for a partially wetting puddle and the location of the static contact angle. J Colloid Interface Sci 348(1):232–239
34. Gaskell PH, Jimack PK, Sellier M, Thompson HM (2004) Efficient and accurate time adaptive multigrid simulations of droplet spreading. Int J Numer Methods Fluids 45(11):1161–1186
35. Koh YY, Lee YC, Gaskell PH, Jimack PK, Thompson HM (2009) Droplet migration: quantitative comparisons with experiment. Eur Phys J Special Topics 166(1):117–120
36. Gomba JM, Homsy GM (2010) Regimes of thermocapillary migration of droplets under partial wetting conditions. J Fluid Mech 647:125–142
37. Oron A, Davis SH, Bankoff SG (1997) Long-scale evolution of thin liquid films. Rev Mod Phys 69:931–980
38. Schwartz LW, Eley RR (1998) Simulation of droplet motion on low-energy and heterogeneous surfaces. J Colloid Interface Sci 202(1):173–188
39. Mitlin VS (1994) On dewetting conditions. Colloid Surf A 89:97–101
40. Bertozzi A, Grün G, Witelski TP (2001) Dewetting films: bifurcations and concentrations. Nonlinearity 14:1569
41. Glasner K, Witelski T (2005) Collision versus collapse of droplets in coarsening of dewetting thin films. Physica D 209:80–104
42. Teletzke GF, Davis H, Scriven LE (1988) Wetting hydrodynamics. Rev Phys Appl 23(6):989–1007
43. Abramowitz M, Stegun IA (1964) Handbook of mathematical functions with formulas, graphs, and mathematical tables. Dover, New York
44. Eggers J (2005) Contact line motion for partially wetting fluids. Phys Rev E 72:061605
45. Savva N, Kalliadasis S (2011) Dynamics of moving contact lines: A comparison between slip and precursor film models. Europhys Lett 94(6):64004
46. Kavehpour HP, Ovryn B, McKinley GH (2003) Microscopic and macroscopic structure of the precursor layer in spreading viscous drops. Phys Rev Lett 91:196104
47. Solomentsev Y, White LR (1999) Microscopic drop profiles and the origins of line tension. J Colloid Interface Sci 218(1):122–136
48. Dörfler F, Rauscher M, Dietrich S (2013) Stability of thin liquid films and sessile droplets under confinement. Phys Rev E 88:012402
49. Perazzo CA, Mac Intyre JR, Gomba JM (2014) Final state of a perturbed liquid film inside a container under the effect of solid–liquid molecular forces and gravity. Phys Rev E 89:043010